HHS Public Access

Author manuscript

Adv Mater. Author manuscript; available in PMC 2024 August 01.

Published in final edited form as:

Adv Mater. 2023 August ; 35(31): e2211717. doi:10.1002/adma.202211717.

Immunostimulatory DNA Hydrogel Enhances Protective Efficacy of Nanotoxoids against Bacterial Infection

Zhongyuan Guo,

Jiarong Zhou Dr.,

Yiyan Yu,

Nishta Krishnan,

Ilkoo Noh Dr.,

Audrey Ting Zhu,

Raina M. Borum Dr.,

Weiwei Gao Dr.,

Ronnie H. Fang Dr.,

Liangfang Zhang Prof.

Department of NanoEngineering, Chemical Engineering Program, and Moores Cancer Center, University of California San Diego, La Jolla, CA 92093

Abstract

While vaccines have been highly successful in protecting against various infections, there are still many high-priority pathogens for which there are no clinically approved formulations. To overcome this challenge, researchers have explored the use of nanoparticulate strategies for more effective antigen delivery to the immune system. Along these lines, nanotoxoids are a promising biomimetic platform that leverage cell membrane coating technology to safely deliver otherwise toxic bacterial antigens in their native form for antivirulence vaccination. Here, in order to further boost their immunogenicity, we embed nanotoxoids formulated against staphylococcal α-hemolysin into a DNA-based hydrogel with immunostimulatory CpG motifs. The resulting nanoparticle–hydrogel composite is injectable and improves the in vivo delivery of vaccine antigens while simultaneously stimulating nearby immune cells. This leads to elevated antibody production and stronger antigen-specific cellular immune responses. In murine models of pneumonia and skin infection caused by methicillin-resistant *Staphylococcus aureus* (MRSA), mice vaccinated with the hybrid vaccine formulation are well protected. This work highlights the benefits of combining nanoparticulate antigen delivery systems with immunostimulatory hydrogels into a single platform, and the approach can be readil generalized to a wide range of infectious diseases.

rhfang@ucsd.edu, Tel: +1-858-246-2773, zhang@ucsd.edu, Tel: +1-858-246-0999.

Conflict of Interest

The authors declare no conflict of interest.

Supporting Information

Supporting Information is available from the Wiley Online Library or from the author.

Graphical Abstract:

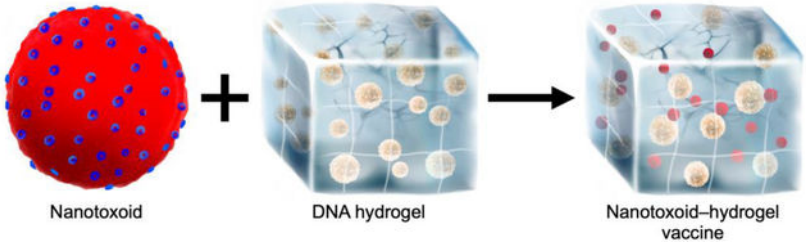

Nanotoxoids formulated against methicillin-resistant *Staphylococcus aureus* are embedded into an immunostimulatory DNA hydrogel. When used to vaccinate mice, the resulting nanoparticle–hydrogel composite effectively elicits antigen-specific humoral and cellular immune responses. This enhanced immunity enables strong protection against live bacterial infection in models of bacterial pneumonia and skin infection.

Keywords

antibiotic-resistant infection; MRSA; nanotoxoid vaccine; nanosponge; biomimetic nanoparticle; DNA origami

Bacterial infection remains one of the leading causes of death around the world, particularly as the widespread use of antibiotics has resulted in the emergence of drug-resistant strains.[1] Methicillin-resistant *Staphylococcus aureus* (MRSA) is an example of a pathogen that has developed resistance against a broad range of antimicrobial drugs and is associated with high mortality rates.[2, 3] With the slow pace of new drug discovery, a greater emphasis has been placed on the development of prophylactic vaccines, which can promote sterilizing immunity to protect against bacterial infections, thus reducing our reliance on antibiotics.[4, 5] Despite the tremendous potential of vaccines, there is currently no clinically approved formulation for MRSA, emphasizing the need for novel vaccine platforms capable of eliciting strong antibacterial immunity.[2, 6] Secreted virulence factors, including various toxins, are utilized by MRSA bacteria to promote their pathogenesis and to circumvent immune surveillance.[7] In contrast to traditional strategies directly targeting bacteria, antivirulence vaccination aims to neutralize these toxic secretions, and this has been shown to offer considerable protection against MRSA infection.[8]

In the past decade, research at the intersection between biomaterials and nanotechnology has yielded exciting new developments that have the potential to significantly benefit vaccine development.[9–11] One emerging platform are cell membrane-coated nanoparticles, which are constructed by a facile top-down process in which synthetic nanoparticulate cores are camouflaged with naturally derived cell membrane.[12] These cell-mimicking nanoparticles have been used for a variety of applications, including the binding and neutralization of biological toxins.[13–15] For antibacterial vaccination, cell membrane-coated nanoparticles can be precomplexed with toxic bacterial antigens to form nanotoxoids, which can then be used as a vaccine to elicit potent antigen-specific immune responses.[16] Traditional toxoids generally require the use of destructive techniques such as heat or chemical treatment in

order to make the final formulation safe for administration.[17, 18] In contrast, nanotoxoids exhibit minimal toxicity while also preserving the original toxin structure, thus striking a favorable balance between safety and antigenicity.[19] Along with the recent interest in biomimetic nanotechnology, DNA-based materials have also received considerable attention in biomedical research, as the predictable nature of base pair hybridization enables the controllable bottom-up synthesis of novel structures that are useful for a wide range of applications.[20] In terms of vaccine design, DNA hydrogels can be naturally incorporated with immunostimulatory motifs, which engage pathogen pattern recognition receptors to induce potent immune responses with the appropriate T helper (Th) cell biasing.[21, 22] As such, the use of nucleic acid-based materials may serve as a powerful approach to augmenting the efficacy of vaccine formulations.[23]

Here, we develop an injectable nanotoxoid-embedded DNA hydrogel as an antivirulence vaccination platform to safely augment the immune response against harmful bacterial antigens and protect against live infection (Figure 1). Staphylococcal α-hemolysin (Hla), a key pore-forming toxin secreted by MRSA, is chosen to prepare the nanotoxoids via insertion into red blood cell membrane-coated nanoparticles. Meanwhile, rolling circle amplification (RCA) is used to synthesize a DNA hydrogel containing immunostimulatory CpG motifs (denoted ‘CpG gel’), which can promote a Th1/Th17-biased immune response that has been identified as important in the control of MRSA infection.[24, 25] In addition, the presence of guanine-rich sequences enable G-quadruplex conformations that form flower-like microstructures within the gel and thus help to stabilize the gel structure.[26] When administered in vivo, the resulting nanotoxoid-loaded CpG hydrogel (denoted ‘NT-CpG gel’) promotes strong immune activation and elicits high levels of Hla-specific IgG titers that protect mice against MRSA pneumonia and skin infection. Overall, the work demonstrates how the rational combination of different biomaterials can yield novel vaccine platforms to aid in the fight against antibiotic resistance.

In order to fabricate the CpG gel by RCA, a linear DNA sequence complementary to CpG 1826 and flanked by cytosine repeats was ligated to produce a circular template. With the help of phi29 DNA polymerase, long single-stranded DNA with hundreds of CpG 1826 repeats and guanine-rich areas was generated. With the help of G-quadruplex formation, the DNA strands were crosslinked to form a hydrogel structure.[26] When using a GelRed stain to aid in visualization, strong fluorescent signal was observed for the CpG gel after RCA, confirming a high concentration of the DNA product (Figure 2a). In contrast, no signal was observed for the reagent mixture prior to the RCA process. Formation of the CpG gel could also be visualized by eye, both without staining and after incubation with propidium iodide (Figure S1, Supporting Information). Importantly, the CpG gel could be easily passed through a syringe with a 29-gauge needle, thus verifying its suitability for injection (Figure 2b). The presence of parallel G-quadruplex structures in the CpG gel formulation was confirmed both by circular dichroism spectroscopy where a weak negative peak around 240 nm and a strong positive peak at 265 nm were observed[26] (Figure 2c), as well as by staining with the fluorescent probe *N*-methyl mesoporphyrin IX[27] (Figure 2d). Concurrently, nanotoxoids against Hla were fabricated as previously described.[16] Briefly, red blood cell (RBC) membrane was purified and then coated onto poly(lactic-*co*-glycolic acid) (PLGA) cores by sonication to prepare RBC membrane-coated nanoparticles

(RBC-NPs). The final nanotoxoids were formed by incubating Hla with the RBC-NPs. As measured by dynamic light scattering, the size of the nanotoxoids was around 95 nm, which was slightly larger than the bare PLGA cores and the RBC-NPs (Figure 2e). The zeta potential of the nanotoxoids was approximately −30 mV, which was similar to that of both the RBC membrane and RBC-NPs (Figure 2f).

To optimize the loading of the nanotoxoids into the CpG gel, the two components were incubated together for increasing amounts of time (Figure 2g). It was observed that the loading efficiency increased progressively with time and plateaued after approximately 2 h at around 90%. For subsequent experiments, all NT-CpG gel samples were prepared using 2 h of incubation. To confirm Hla loading, dot blot analysis was performed, and it was shown that the toxin was highly present in both the nanotoxoid and NT-CpG gel samples, whereas no signal was detected for the unloaded RBC-NPs (Figure 2h). The morphology of the NT-CpG gel was visualized using scanning electron microscopy, which revealed densely packed flower-like microstructures similar to what others have reported previously[26] (Figure 2i). Rheological analysis confirmed the successful formation of a hydrogel structure, [28] with relatively low storage and loss moduli values suggesting favorable injectability properties for both the CpG gel and NT-CpG gel formulations[29] (Figure 2j). Compared with the CpG gel formulation, the NT-CpG gel exhibited moderately higher storage and loss moduli, potentially relating to adhesive interactions between the CpG gel and nanotoxoids. [30] To measure the amount of CpG 1826 within the CpG gel, the restriction enzyme HaeIII was utilized to specifically digest the long DNA strands into individual small units; successful digestion was confirmed using agarose gel electrophoresis (Figure 2k). Using DNA oligonucleotides synthesized to match the HaeIII-digested sequence as a standard (Figure S2, Supporting Information), we measured that one 50-μL scale synthesis of the CpG gel contained approximately 9.1 nmol of CpG 1826. To explore the degradation of the CpG gel in solution, GelRed labeling was performed followed by incubation at 37 °C (Figure 2l; Figure S3, Supporting Information). Both by visualization and quantitative analysis, it was observed that the CpG gel was highly stable in solution, and considerable degradation was observed only after the addition of the HaeIII restriction enzyme at 8 h. We next explored the release of dye-labeled nanotoxoids from the NT-CpG gel over 24 h at 37 °C using a transwell setup (Figure 2i). It was observed that, after 1 h of incubation, there was a burst release of 30%, after which the kinetics leveled off. To confirm that all of the nanotoxoids could be released, a separate NT-CpG gel sample was treated with HaeIII at 8 h after the start of the experiment. At this point, the kinetics rapidly accelerated until approximately 100% nanotoxoid release was achieved by the 24 h experimental endpoint.

After successful preparation of the NT-CpG gel, we first confirmed the safety of the formulation in vitro. When incubated with RBCs, minimal hemolysis was observed, indicating that the Hla remained neutralized when incorporated into the CpG gel (Figure 3a). Similarly, there was minimal cytotoxicity when incubating the NT-CpG gel with bone marrow-derived dendritic cells (BMDCs), as determined by annexin V and propidium iodide staining (Figure 3b). We next studied how formulating the nanotoxoids within the CpG gel would affect their uptake by BMDCs (Figure 3c–e). Using dye-labeled RBC-NPs, it was observed that the cells internalized free nanotoxoids much more quickly compared with nanotoxoids in the NT-CpG gel over the first 2 days, after which the trend was

slightly reversed. This highlighted the sustained release characteristics of the NT-CpG gel formulation, suggesting that the incorporation of nanotoxoids into a DNA-based hydrogel could help to prolong antigen exposure for vaccine applications.

Given the ability of CpG 1826 to serve as a Toll-like receptor (TLR) 9 agonist,[31, 32] we proceeded to evaluate the immunostimulatory activity of the NT-CpG gel in vitro. As a control, a non-stimulatory gel containing the CpG 1826 sequence, but with all CpG motifs replaced with GpC motifs, was fabricated (denoted 'GpC gel'). When incubated with BMDCs, the CpG gel was able to significantly elevate the expression of the maturation markers CD40, CD80, CD86, and major histocompatibility complex II (MHC-II), whereas the GpC gel was unable to activate the cells (Figure S4, Supporting Information). The NT-CpG gel formulation was also able to induce strong dendritic cell maturation, confirming that the loading of nanotoxoids did not impact the CpG gel's capacity for immune stimulation. When comparing with controls of free nanotoxoids and a nanotoxoid-loaded GpC gel (denoted 'NT-GpC gel'), only the NT-CpG gel enhanced the expression of BMDC maturation markers (Figure 3f–i) and the secretion of the proinflammatory cytokines interleukin (IL)-6 and IL-12p40 (Figure 3j,k). Considering that synthetic CpG oligonucleotides are generally fabricated with phosphorothioate (PS) bonds instead of phosphodiester (PO) bonds to prevent nuclease degradation,[33, 34] we were curious whether or not the CpG gel would be negatively impacted by the fact that our RCA process could only yield PO-bonded DNA. As such, we compared the immunostimulatory activity of free CpG 1826 containing PS or PO bonds with that of the CpG gel, either by itself or formulated with nanotoxoids (Figure S5, Supporting Information). Neither of the samples containing the free PO-bonded CpG 1826 demonstrated activity in vitro, whereas all samples with either the PS-bonded CpG 1826 or the CpG gel were highly effective at promoting BMDC activation. This indicated that, despite its PO bonds, the supramolecular structure of the CpG gel was likely able to prevent its rapid degradation, thus preserving its ability to act as a TLR agonist.

To explore how the NT-CpG gel formulation physically changed over time in vivo, samples were labeled with GelRed and injected subcutaneously (Figure 4a,b). Recovery of the gel at increasing timepoints revealed a time-dependent degradation profile, with approximately 80% and 10% of the original gel remaining after 1 and 6 days, respectively. Considering the sustained release of nanotoxoids from the NT-CpG gel in vitro, we wanted to confirm if the DNA-based hydrogel could also facilitate improved retention and delivery after in vivo administration. Accordingly, mice were subcutaneously injected with the same dose of dye-labeled nanotoxoids either in free form or within the NT-CpG gel formulation, followed by live imaging over the course of 6 days (Figure 4c). The CpG gel significantly enhanced the retention of the nanotoxoids, likely by preventing them from freely transporting away from the injection site. As a vaccination platform, it is also important for the nanotoxoids to eventually be delivered into lymph organs, where they can be processed by resident antigen-presenting cells. To study this, mice were subcutaneously administered in the hock region with the same dye-labeled formulations, and the draining popliteal lymph nodes were collected on days 2, 3, and 4 for analysis (Figure 4d,e). Compared with free nanotoxoids, administration of the NT-CpG gel resulted in higher fluorescence in the lymph nodes at each timepoint, with the signal peaking on day 3. To further identify the exact cell populations

interacting with the nanotoxoids, the lymph nodes collected on day 3 were dissociated into single-cell suspensions and analyzed by flow cytometry (Figure 4f). The highest degree of uptake was observed among antigen-presenting cells, including macrophages, B cells, and dendritic cells; in each case, the percentage of cells positive for nanotoxoid uptake was significantly higher for the NT-CpG gel group compared with the free nanotoxoid group.

In order to characterize in vivo immune responses, mice were subcutaneously vaccinated with free nanotoxoids or the NT-CpG gel, and organ samples were collected at various timepoints for analysis. At 48 h, it was observed that the NT-CpG gel induced the highest degree of dendritic cell maturation in the draining lymph nodes as determined by CD40, CD80, and CD86 expression (Figure 5a–c). To explore the impact of vaccination on the formation of germinal centers, which are essential for the production of long-lived plasma cells and memory B cells against infection,[35] the draining popliteal lymph nodes were collected after 21 days (Figure 5d; Figure S6, Supporting Information). Both flow cytometry and immunofluorescence staining of histological sections confirmed that the NT-CpG gel outperformed free nanotoxoids in terms of eliciting B cells with a $GL7^+$ germinal center phenotype. To study antigen-specific T cell responses, which have been identified to be important for the clearance of bacterial infections,[24, 36] splenocytes derived from mice 28 days after vaccination were restimulated with Hla (Figure 5e–g). The levels of interferon γ (IFN-γ) and IL-17A were significantly elevated in the NT-CpG gel group after 5 days of stimulation, indicating that the CpG motifs were able to provide a bias towards Th1 and Th17 immunity.[37] In contrast, IL-4 levels were not significantly different from baseline levels. Finally, the ability of the NT-CpG gel formulation to elicit toxin-specific antibodies was evaluated by sampling the serum 35 days after subcutaneous vaccination (Figure 5h). While free nanotoxoids were reasonably efficient at eliciting anti-Hla IgG titers,[16, 38] the NT-CpG gel elevated titer levels even further. Hla-specific antibody levels in the serum remained high for at least 2 months after NT-CpG gel vaccination (Figure S7, Supporting Information). Interestingly, free nanotoxoids co-administered with free PS-bonded CpG 1826 also induced high antibody production against Hla on par with the NT-CpG gel, but the antigen-specific cellular responses were weaker (Figure S8, Supporting Information). To further explore the ability of the NT-CpG gel to promote long-term immunity, memory immune cell populations in the draining lymph nodes were detected (Figure 5i–m). It was observed that memory B cells, $CD4^+$ effector memory T cells, and $CD8^+$ central memory T cells, all of which can be important in defending against infections, were significantly elevated in mice receiving the NT-CpG gel formulation.[39–41]

To investigate the protective efficacy of NT-CpG gel vaccination against MRSA, we employed murine models of MRSA pneumonia and skin infection. Mice were vaccinated once with free nanotoxoids or the NT-CpG gel, followed by bacterial challenge on day 35. For the pneumonia model, mice were intratracheally instilled with live MRSA, and lung tissues were collected after 1 day to enumerate the bacterial load (Figure 6a). Whereas the free nanotoxoids modestly reduced disease burden, NT-CpG gel vaccination offered significantly better protection, reducing bacterial counts by nearly 3 orders of magnitude. This result correlated well with anti-Hla IgG titers in the lungs after bacterial challenge, which were the most elevated in mice receiving the NT-CpG gel (Figure 6b). For the skin infection model, mice were subcutaneously challenged with MRSA, and lesion sizes were

monitored over time (Figure 6c). Again, the NT-CpG gel offered the best protection, with the area of the lesions remaining significantly smaller compared with those of free nanotoxoid-vaccinated mice. On day 6 after the skin challenge, the infected skin area was collected and homogenized for bacterial enumeration (Figure 6d). The results here correlated well with the skin lesion data, with the NT-CpG gel group showing significantly lower bacterial counts compared to the free nanotoxoid group. This was also reflected in the bacterial counts for individual organs, including the kidneys, heart, liver, lungs, and spleen, which indicated that mice vaccinated with the NT-CpG gel had the lowest systemic exposure to MRSA after the skin infection (Figure 6e). The NT-CpG gel formulation also outperformed free nanotoxoids co-administered with free PS-bonded CpG 1826 (Figure S9, Supporting Information), suggesting that maximal bacterial clearance was mediated by a combination of both strong humoral and cellular immunity. To further explore the cellular mechanisms behind the protective efficacy elicited by the NT-CpG gel formulation, mice were vaccinated and then challenged with MRSA after 21 days. Infected skin samples were collected on day 3 post MRSA challenge for immune cell profiling[42] (Figure 6f–p). Overall, NT-CpG gel vaccination was effective at enhancing the infiltration of T cells, including Th1, Th2, and Th17 subsets, as well as M1 type macrophages, indicating a combination of both innate and adaptive cellular immunity working together to help clear the MRSA infection.

In summary, we have developed an immunostimulatory DNA hydrogel containing a high number of CpG oligonucleotide repeats that can be readily loaded with biomimetic nanotoxoids to elicit strong protective immunity against bacterial infection. The final NT-CpG gel formulation improved the in vivo retention and delivery of its nanotoxoid payload while efficiently stimulating antigen-presenting cells. This resulted in strong adaptive immunity, which included the high production of Hla-specific IgG titers and augmented cellular immune responses. Vaccination of mice with the NT-CpG gel offered significant protection from live MRSA challenge in models of pneumonia and skin infection. Overall, the work presented here highlights the considerable benefits of leveraging nanoparticle–hydrogel superstructures for biomedical applications.[43, 44] Whereas the administration of free bacterial toxins would cause significant harm to a host, the nanotoxoid component provided an effective means of safely and faithfully delivering otherwise toxic antigenic payloads in a format that is easily processed by immune cells. At the same time, the DNA hydrogel was engineered to be inherently immunostimulatory while also helping to prolong the retention of the nanotoxoids. In the future, either component can be modulated to generalize this approach for other diseases and applications. For example, the specificity of the nanotoxoid can be altered by using a different membrane coating combined with antigenic material from other pathogens.[45, 46] For the hydrogel component, various types of nucleic acid-based structures can be designed with custom-tailored functionality.[47, 48] Continued research along these lines will yield new platforms with unique features that can be used to help address a wide range of important human health conditions.

Experimental Section

Animal Care.

Six-week-old male CD1 mice were purchased from Envigo and housed in an animal facility at the University of California San Diego (UCSD) under federal, state, and local guidelines. All animal experiments were performed in accordance with National Institutes of Health guidelines and approved by the Institutional Animal Care and Use Committee (IACUC) of UCSD.

CpG Gel Preparation.

All primers and templates (Table S1) were synthesized by Eton Bioscience and dissolved at 100 μM in DNase/RNase-free distilled water (Invitrogen). For the ligation process, 8 μL of the primer, 0.8 μL of the template, and 5 μL of T4 DNA ligase reaction buffer (New England Biolabs) were mixed with 36.2 μL of water and heated at 90 °C for 10 min, followed by gradual cooling to room temperature in a Bio-Rad DNA Engine Dyad thermal cycler. Then, 1 μL of T4 DNA ligase (New England Biolabs) was added into the annealed mixture and incubated at 16 °C for 16 h. The enzyme was inactivated at 65 °C for 10 min. For the RCA process, to make 50 μL of the CpG gel, 10 μL of freshly prepared ligation product was mixed with 10 μL of 10 mM deoxynucleotide solution mix (New England Biolabs), 5 μL of phi29 DNA polymerase reaction buffer (New England Biolabs), 1 μL of phi29 DNA polymerase (New England Biolabs), and 24 μL of water, followed by heating at 30 °C for 24 h and inactivation at 85 °C for 10 min. To facilitate visual observation, 1 μL of propidium iodide solution (BioLegend) was added to 50 μL of the CpG gel. For fluorescence visualization, 1 μL of GelRed stock (excitation/emission = 280/590 nm, Biotium) was added into either 50 μL of the reagent mixture prior to RCA or the final CpG gel product. After 2 h of incubation at 4 °C, imaging was performed under an ultraviolet light in a Bio-Rad Universal Hood II Gel Doc system. The injectability of the CpG gel was confirmed with a 29-gauge insulin syringe (EXELINT).

To detect G-quadruplex formation, a CpG gel was prepared at a 300-μL scale, and its circular dichroism spectrum was measured using a Jasco J-715 CD spectrometer. For *N*-methyl mesoporphyrin IX (excitation/emission = 399/610 nm, Cayman Chemical) staining, 1 μL of a 2.5 mM reagent solution was added into 50 μL of a CpG gel. As controls, a CpG gel reagent mixture before RCA and a non-G-quadruplex CpG gel were prepared. Stained samples were stored at 4 °C for 24 h, and the fluorescence was then detected using a BioTek Synergy MX microplate reader.

To image the degradation of CpG gels, 1 μL of GelRed stock was added into 50 μL of a CpG gel. After 24 h of incubation at 4 °C, the GelRed-labeled CpG gels were transferred into a 96-well plate with 100 μL of PBS and further incubated at 37 °C. At predetermined timepoints, the CpG gels were imaged using a Bio-Rad ChemiDoc MP imaging system. For restriction enzyme treatment, 100 μL of 0.2 U/μL HaeIII (New England Biolabs) in rCutSmart buffer (New England Biolabs) was used instead of PBS starting at 8 h of incubation. To quantify the degree of degradation, GelRed-labeled CpG gels were placed into 5.0-μm pore polycarbonate membrane transwell inserts (Corning) in an untreated

24-well plate (Genesee Scientific) containing 500 μL of PBS per well. At predetermined timepoints, the solution in the well outside of the insert was collected for fluorescence measurements on a Tecan Spark 20M multimode microplate reader. For HaeIII treatment, 500 μL of 0.2 U/μL HaeIII was used instead of PBS starting at 8 h of incubation.

Nanotoxoid Preparation.

Nanotoxoids were prepared according to a previously reported procedure.[38] Briefly, 1 mL of 10 mg/mL 0.66 dL/g carboxyl-terminated PLGA (LACTEL Absorbable Polymers) in acetone was added into 2 mL of water and evaporated under vacuum for 2.5 h to prepare the cores. To facilitate nanoparticle tracking, dye-labeled PLGA cores were also fabricated using either 0.1 wt% 1,1'-dioctadecyl-3,3,3',3'-tetramethylindodicarbocyanine (DiD; excitation/emission = 644/665 nm, Invitrogen) or 1,1'-dioctadecyl-3,3,3',3'-tetramethylindotricarbocyanine (DiR; excitation/emission = 750/780 nm, Invitrogen). RBC membrane was extracted from mouse RBCs by multiple rounds of hypotonic treatment. For membrane coating, the PLGA cores and RBC membrane were mixed at a 4:1 polymer to protein weight ratio and sonicated for 2 min in a Fisher Scientific FS30D bath sonicator. The resulting RBC-NPs were then incubated with Hla (Sigma-Aldrich) at room temperature for 2 h at a 200:3 polymer to Hla weight ratio, and the final nanotoxoid product was adjusted to 1× phosphate buffered saline (PBS) with a 20× PBS stock (Teknova). All nanotoxoid concentrations are expressed in terms of PLGA weight. Size and zeta potential were measured by dynamic light scattering using a Malvern Zetasizer Nano ZS90.

NT-CpG Gel Fabrication.

To fabricate the NT-CpG gel, 10 μL of nanotoxoids at 2.5 mg/mL was added into 50 μL of the CpG gel, followed by incubation for 2 h at 4 °C. Unless explicitly specified, all in vitro and in vivo experiments employed one batch of NT-CpG gel fabricated at this scale per replicate. Controls utilized equivalent amounts of Hla, free nanotoxoids, free CpG 1826, or DNA gels where appropriate. To quantify loading efficiency, DiR-labeled nanotoxoids were incubated with the CpG gel for increasing amounts of time, after which the gel was gently transferred into 1 mL of PBS for 3 min and then removed. The fluorescence in the remaining solution was measured using a Tecan Spark 20M multimode microplate reader.

NT-CpG Gel Characterization.

For dot blot analysis, nanotoxoids prepared by mixing 133 μg of RBC-NPs with 2 μg of Hla were added into 50 μL of the CpG gel, followed by 2 h of incubation. The resulting NT-CpG gel was then washed once with 1 mL of PBS and digested using 0.2 U/μL of HaeIII for 2 h. Free Hla, RBC-NPs, nanotoxoids, and the digested NT-CpG gel were prepared with NuPAGE LDS sample buffer (Invitrogen) and heated at 70 °C for 10 min. Then, 1 μL samples were spotted onto a nitrocellulose membrane (Thermo Scientific). After drying, the membrane was blocked with 5% nonfat dry milk (Apex) and 1% bovine serum albumin (BSA; Sigma-Aldrich) in PBS containing 0.05% Tween 20 (National Scientific) (PBST) for 1 h at room temperature. After incubation with a polyclonal anti-staphylococcal α-toxin (S7531, Sigma-Aldrich) at 4 °C for 16 h followed by a horse radish peroxidase (HRP)-conjugated anti-rabbit (BioLegend) at room temperature for 2 h, the blot was developed on film using Pierce ECL western blotting substrate (Thermo Scientific). For scanning electron

microscopy visualization, 5 μL of the NT-CpG gel was deposited onto a 0.5 cm × 0.5 cm silicon wafer (UniversityWafer) and frozen at −80 °C for 1 h before lyophilization using a Labconco FreeZone 4.5 freeze drier for 48 h. After 12 s of sputter coating with iridium on an Emitech K575X Sputter Coater, the images were acquired using a Zeiss Sigma 500 field-emission scanning electron microscope at a beam energy of 1 kV. For rheological analysis, 50 μL of a CpG gel or an NT-CpG gel was loaded onto an 8.0 mm ETC stainless steel parallel plate and measured using a TA Instruments Discovery HR30 hybrid rheometer at the UC San Diego Materials Research Science and Engineering Center supported by the U.S. National Science Foundation grant DMR-2011924. The measurement was performed in oscillation frequency mode where the temperature was kept at 23 °C and the strain was 25.0%.

To measure the concentration of CpG 1826, the NT-CpG gel was incubated with 0.2 U/μL of HaeIII for 24 h at 37 °C. To confirm successful digestion, samples before and after the digest were prepared with purple gel loading dye (New England Biolabs) and subjected to electrophoresis on a 3% agarose (Apex) gel at 100 V for 1 h. A Quant-iT OliGreen ssDNA assay kit (Invitrogen) was used to determine the CpG 1826 concentration using an oligonucleotide with the predicted HaeIII-digested sequence (Table S1) synthesized by Eton Bioscience as the standard. To measure nanotoxoid release, an NT-CpG gel made with DiR-labeled nanotoxoids was placed into a 5.0-μm pore polycarbonate membrane transwell insert in an untreated 24-well plate containing 500 μL of PBS per well. At predetermined timepoints, the solution in the well was collected for fluorescence measurements on a Tecan Spark 20M multimode microplate reader and replaced with 500 μL of fresh PBS. For restriction digest treatment, 500 μL of 0.2 U/μL HaeIII was used instead of PBS starting at 8 h of incubation.

In Vitro Safety Studies.

To evaluate hemolysis, 60 μL of 2.5% mouse RBCs was mixed with an equal volume of Hla, nanotoxoids, or an NT-CpG gel at an Hla concentration of 6.25 μg/mL, followed by incubation at room temperature for 15 min. After spinning down any intact RBCs at 3000 *g* for 5 min, the supernatant was collected, and absorbance was measured at 540 nm using a Tecan Spark 20M multimode microplate reader. To evaluate cytotoxicity, BMDCs were first collected from CD1 mice following a previously established protocol[49] and cultured in BMDC media formulated by supplementing 500 mL of Iscove's modified Dulbecco's medium with 2 mM L-glutamine and 25 mM HEPES (Gibco) with 5 mL of 200 mM L-glutamine (Gibco), 500 μL of 55 mM 2-mercaptoethanol (Gibco), 5 mL of penicillin-streptomycin (Gibco), and 50 mL of USDA-approved fetal bovine serum (Gibco), followed by the addition of granulocyte-macrophage colony-stimulating factor (BioLegend) at a final concentration of 10 ng/mL. For the study, BMDCs were seeded at 400,000 cells per well into an untreated 12-well plate. After overnight incubation, nanotoxoids or an NT-CpG gel was added for 48 h. The cells were then collected with 1 mM ethylenediaminetetraacetic acid (EDTA) in PBS diluted from a 0.5 M EDTA stock (Corning). After two washes with PBS, the cells were stained with 5 μL of FITC-labeled annexin V (BioLegend) and 10 μL of propidium iodide per 100,000 cells in 100 μL of annexin V binding buffer (BioLegend).

Data were acquired using a Becton Dickinson LSR II flow cytometer, and the percentage of live cells double negative for the two stains was determined using FlowJo software.

In Vitro Uptake and Immune Activation Studies.

BMDCs were seeded at 400,000 cells per well into an untreated 12-well plate, followed by incubation with DiD-labeled nanotoxoids in free form or within an NT-CpG gel. Cells were collected with 1 mM EDTA in PBS at predetermined timepoints and analyzed by flow cytometry. Data were acquired using a Becton Dickinson LSR II flow cytometer, and the mean fluorescence intensity of the cells was determined using FlowJo software. To assess immune activation, BMDCs were seeded at 400,000 cells per well into an untreated 12-well plate, followed by incubation with nanotoxoids, PO-bonded CpG 1826, PS-bonded CpG 1826, a GpC gel, a CpG gel, nanotoxoids plus PO-bonded CpG 1826, nanotoxoids plus PS-bonded CpG 1826, an NT-GpC gel, or an NT-CpG gel for 48 h. For cytokine analysis, 200 μL of the culture medium was collected for detection of IL-6 and IL-12p40 by ELISA using the appropriate kits (BioLegend) according to the manufacturer's instructions. For flow cytometry, the cells were collected with 1 mM EDTA in PBS and washed twice with PBS before staining with a LIVE/DEAD fixable aqua dead cell stain kit (Invitrogen). Then, cells were blocked with 1% BSA in PBS for 30 min and stained with PE/cyanine7 anti-mouse CD11c (N418, BioLegend), APC/Fire 750 anti-mouse F4/80 (BM8, BioLegend), PerCP anti-mouse I-A/I-E (M5/114.15.2, BioLegend), FITC anti-mouse CD40 (HM40–3, BioLegend), PE anti-mouse CD80 (16–10A1, BioLegend), and Alexa Fluor 647 anti-mouse CD86 (GL-1, BioLegend). Unstained and single-stained controls were used for compensation and gating purposes. Data were acquired using a Becton Dickinson LSR II flow cytometer and analyzed using FlowJo software. The $CD11c^{+}F4/80^{-}$ population was selected prior to analyzing maturation marker expression.

In Vivo Delivery Studies.

To observe morphological changes in vivo over time, NT-CpG gels were first labeled with GelRed, followed by subcutaneous injection into the neck region of mice. At predetermined timepoints, the mice were euthanized, and the NT-CpG gels were recovered for imaging using a Bio-Rad ChemiDoc MP imaging system. The amount of GelRed signal was quantified using ImageJ. To evaluate retention, mice were shaved in the flank area and then injected subcutaneously with DiR-labeled nanotoxoids in free from or within an NT-CpG gel. At various timepoints, the mice were anesthetized with isoflurane, and the fluorescence at the injection site was imaged and measured using a PerkinElmer Xenogen IVIS 200 imaging system. To track delivery to the lymph nodes, mice were injected subcutaneously at the hock region with DiD-labeled nanotoxoids in free from or within an NT-CpG gel. After 2, 3, and 4 days, groups of mice were euthanized, and their draining popliteal lymph nodes were collected, followed by fluorescence imaging and quantification using a PerkinElmer Xenogen IVIS 200 imaging system. To explore the uptake by different immune cell populations, the draining popliteal lymph nodes were collected 3 days after injection with DiD-labeled nanotoxoids in free from or within an NT-CpG gel and manually dissociated. After passing the tissue through Flowmi 40-μm cell strainers (Bel-Art), the single-cell suspensions were washed twice with PBS and then stained with a LIVE/DEAD fixable aqua dead cell stain kit. The cells were then blocked with 1% BSA in PBS for

30 mins and stained with PE/cyanine7 anti-mouse CD11c, FITC anti-mouse CD3 (17A2, BioLegend), Pacific Blue anti-mouse CD19 (6D5, BioLegend), APC/cyanine7 anti-mouse CD11b (M1/70, BioLegend), PE anti-mouse F4/80 (BM8, BioLegend), and PerCP anti-mouse Ly-6G/Ly-6C (Gr-1) (RB6–8C5, BioLegend). Unstained and single-stained controls were used for compensation and gating purposes. Data were acquired using a Becton Dickinson LSR II flow cytometer and analyzed using FlowJo software. Different cell populations, including T cells ($CD3^+$), B cells ($CD19^+$), dendritic cells ($CD11c^+F4/80^-$), macrophages ($CD11b^+F4/80^+$), and granulocytes ($CD11b^+Gr\text{-}1^+$), were gated prior to analyzing for DiD signal.

In Vivo Immune Activation Studies.

To assess for in vivo dendritic cell maturation, mice received a subcutaneous injection in the hock region with nanotoxoids or an NT-CpG gel. The draining popliteal lymph nodes were then collected after 48 h and processed into single-cell suspensions as before. Expression of CD40, CD80, and CD86 was analyzed in the same manner as described above for the in vitro study. To assess for germinal center formation, mice were vaccinated with nanotoxoids or an NT-CpG gel at the hock region, and the draining popliteal lymph nodes were collected 21 days after vaccination. After the preparation of single-cell suspensions, the cells were washed and stained with a LIVE/DEAD fixable aqua dead cell stain kit. The cells were then blocked with 1% BSA in PBS and further stained with Pacific Blue anti-mouse/human CD45R/B220 (RA3–6B2, BioLegend) and Alexa Fluor 647 anti-mouse/human GL7 (GL7, BioLegend). Data were acquired using a Becton Dickinson LSR II flow cytometer and analyzed using FlowJo software. Germinal center B cells were gated as the $B220^+GL7^+$ population. For germinal center imaging, the draining popliteal lymph nodes were collected 21 days after vaccination, snap frozen in Tissue-Tek O.C.T. compound (Sakura) at −80 °C, and cryosections were prepared by the Moores Cancer Center Tissue Technology Shared Resource (Cancer Center Support Grant P30CA23100). The sections were then blocked with 1% BSA in PBS and stained with the same antibodies as above, followed by imaging on a Keyence BZ-X710 fluorescence microscope.

Antigen-Specific Cellular Immune Responses.

For the splenocyte restimulation study, mice were vaccinated with nanotoxoids, nanotoxoids plus PO-bonded CpG 1826, nanotoxoids plus PS-bonded CpG 1826, an NT-GpC gel, or an NT-CpG gel at the hock region. After 28 days, the spleens were collected into the sterile PBS containing 1 mg/mL of collagenase D (Roche) and 1 mg/mL of DNase I (Roche). The tissues were mechanically dissociated and then filtered through 70-μm cell strainers (Fisher Scientific). After treatment with RBC lysis buffer (BioLegend) per the manufacturer's instructions, the splenocytes were cultured in untreated 6-well plates (GenClone) with 4 million cells in 2 mL of BMDC media per well containing Hla at a final concentration of 50 ng/mL. After 5 days, 200 μL of the culture media was collected for the detection of IFN-γ, IL-17A, and IL-4 using the appropriate ELISA kits (BioLegend).

Detection of Antibody Titers.

To quantify antigen-specific IgG antibody production, mice were vaccinated subcutaneously in the neck region with nanotoxoids, nanotoxoids plus PO-bonded CpG 1826, nanotoxoids

plus PS-bonded CpG 1826, an NT-GpC gel, or an NT-CpG gel. After 35 days, the sera from the mice were collected for analysis by indirect ELISA. In a separate experiment, serum samples were collected over time after NT-CpG gel vaccination. For the analysis, 96-well assay plates (Corning) were coated with 2 μg/mL of Hla using ELISA coating buffer (BioLegend) at 4 °C for 16 h. After blocking with buffer consisting of 5% milk and 1% BSA in PBST, serum samples serially diluted in the blocking buffer were loaded onto the plates, followed by incubation at room temperature for 2 h. Plates were then incubated with HRP-conjugated anti-mouse IgG (BioLegend) for 2 h and developed with TMB substrate (BioLegend); the reaction was stopped with 1 N HCl. The absorbance at 450 nm was measured using a Tecan Spark 20M multimode microplate reader. To detect Hla-specific IgG titers in the lungs, 1 day after vaccinated mice were intratracheally challenged with live MRSA as described in the following section, the organs were collected and homogenized in PBS with 2-mm zirconia beads (BioSpec) using a BioSpec Mini-BeadBeater-16. The homogenate was spun down at 10,000 *g* for 10 min and filtered through 0.22-μm PVDF syringe filters (CellTreat). Titers were assayed by indirect ELISA as described above. The absorbance data were fitted to a four-parameter logistic curve, and titer levels were interpolated using GraphPad Prism 8.

Detection of Memory Immune Cells.

Mice were vaccinated subcutaneously in the neck region with nanotoxoids or an NT-CpG gel, and the axillary lymph nodes were collected on day 28 and processed into single-cell suspensions as before. The cells were then washed with PBS and stained with a LIVE/DEAD fixable aqua dead cell stain kit before blocking with 1% BSA in PBS. To detect memory B cells, the cell suspension was further stained with PE/Dazzle 594 anti-mouse CD45 (30-F11, BioLegend), Pacific Blue anti-mouse CD19, and PE/cyanine7 anti-mouse CD73 (TY/11.8, BioLegend). To detect memory T cells, the cell suspension was further stained with PE/Dazzle 594 anti-mouse CD45, FITC anti-mouse CD3, APC/Fire750 anti-mouse CD4 (GK1.5, BioLegend), Pacific Blue anti-mouse CD8a (53–6.7, BioLegend), PE anti-mouse/human CD44 (IM7, BioLegend), PE/cyanine7 anti-mouse CCR7 (4B12, BioLegend), and APC anti-mouse CD62L (MEL-14, BioLegend). Data were acquired using a Becton Dickinson LSR II flow cytometer and analyzed using FlowJo software.

Protection Against Live Bacterial Infection.

MRSA USA300 (BAA-1717; American Type Culture Collection) was cultured in tryptic soy broth (Sigma-Aldrich) and washed twice with PBS by centrifuging at 3000 *g* before use. For the pneumonia model, mice were vaccinated subcutaneously in the neck with nanotoxoids or an NT-CpG gel, and the challenge was performed after 35 days by intratracheally instilling 3×10^7 CFU of MRSA. At 24 h post challenge, the mice were euthanized, and their lungs were collected and homogenized with 2-mm zirconia beads using a BioSpec Mini-BeadBeater-16. For bacterial enumeration, the homogenates were diluted serially and plated onto tryptic soy agar (Becton Dickinson) for 20 h at 37 °C before the colonies were counted. For the skin infection model, mice were vaccinated subcutaneously in the neck region with nanotoxoids, nanotoxoids plus PO-bonded CpG 1826, nanotoxoids plus PS-bonded CpG 1826, an NT-GpC gel, or an NT-CpG gel, and the challenge was performed after 35 days by subcutaneously injecting 1×10^9 CFU of MRSA into a shaved flank area. The lesions

were measured daily with a caliper, and their areas were calculated as length × width. On day 6 after the challenge, the mice were euthanized, and the affected skin area, as well as the kidneys, heart, liver, lungs, and spleen, were collected and homogenized for bacterial enumeration.

Immune Cell Profiling in Infected Skin.

Mice were vaccinated subcutaneously in the neck with nanotoxoids or an NT-CpG gel, followed by challenge with MRSA on day 21 as described above. On day 3 after the MRSA challenge, the mice were euthanized, and infected skin samples were collected. The tissues were first incubated in 1 mL of RPMI 1640 (Gibco) supplemented with 10% fetal bovine serum, 10 mM HEPES, and 1% penicillin-streptomycin at 37 °C for 30 min. They were then cut into small pieces and digested in 1 mL of RPMI 1640 containing 1 mg/mL collagenase D and 1 mg/mL DNase I at 37 °C for 30 min, followed by filtration through 70-μm cell strainers. The resulting single-cell suspensions were washed with PBS and divided into three groups. Each was first stained with a LIVE/DEAD fixable aqua dead cell stain kit, blocked with 1% BSA in PBS, and further blocked with TruStain FcX PLUS anti-mouse CD16/32 antibody (S17011E, BioLegend). For the detection of T cells and the various Th cell subsets, subsequent staining was performed with PE/Dazzle 594 anti-mouse CD45, FITC anti-mouse CD3, and APC/Fire750 anti-mouse CD4, followed by treatment with True-Nuclear transcription factor buffer (BioLegend) and further staining with PE/cyanine7 anti-T-bet (4B10, BioLegend), PerCP/cyanine5.5 anti-GATA3 (16E10A23, BioLegend), and PE anti-mouse RORγt (Q31–378, BD Biosciences). For the detection of neutrophils and macrophages, subsequent staining was performed with PE/Dazzle 594 anti-mouse CD45, PerCP/cyanine5.5 anti-mouse Ly-6G (1A8, BioLegend), APC/Fire 750 anti-mouse F4/80, and APC anti-mouse CD38 (90, BioLegend), followed by treatment with True-Nuclear transcription factor buffer and further staining with PE anti-mouse Egr2 (erongr2, Invitrogen). For the detection of all other immune cells, subsequent staining was performed with PE/Dazzle 594 anti-mouse CD45, Pacific Blue anti-mouse CD19, APC anti-mouse CD11c (N418, BioLegend), and PE anti-mouse NK1.1 (PK136, BioLegend). Data were acquired using a Becton Dickinson LSR II flow cytometer and analyzed using FlowJo software.

Statistical Analysis.

All data were analyzed using GraphPad Prism 8. For studies with two groups, statistical significance was determined using an unpaired two-tailed Student's *t*-test. For studies with more than two groups, statistical significance was determined using ordinary one-way ANOVA with Tukey's multiple comparisons test (all groups compared with each other) or Dunnett's multiple comparisons test (all groups compared with NT-CpG gel). Each group had a minimum sample size of 3. Data are presented as the mean ± standard deviation (SD).

Supplementary Material

Refer to Web version on PubMed Central for supplementary material.

Acknowledgements

This work is supported by the Defense Threat Reduction Agency Joint Science and Technology Office for Chemical and Biological Defense under Grant Numbers HDTRA1-18-1-0014 and HDTRA1-21-1-0010 and the National Institutes of Health under Award Number R21AI159492.

References

[1]. Antimicrobial Resistance Collaborators Lancet 2022, 399, 629.

[2]. Turner NA, Sharma-Kuinkel BK, Maskarinec SA, Eichenberger EM, Shah PP, Carugati M, Holland TL, Fowler VG, Nat. Rev. Microbiol. 2019, 17, 203. [PubMed: 30737488]

[3]. Lee AS, De Lencastre H, Garau J, Kluytmans J, Malhotra-Kumar S, Peschel A, Harbarth S, Nat. Rev. Dis. Primers 2018, 4, 1. [PubMed: 29930242]

[4]. Micoli F, Bagnoli F, Rappuoli R, Serruto D, Nat. Rev. Microbiol. 2021, 19, 287. [PubMed: 33542518]

[5]. Klugman KP, Black S, Proc. Natl. Acad. Sci. U.S.A. 2018, 115, 12896. [PubMed: 30559195]

[6]. Giersing BK, Dastgheyb SS, Modjarrad K, Moorthy V, Vaccine 2016, 34, 2962. [PubMed: 27105559]

[7]. Algammal AM, Hetta HF, Elkelish A, Alkhalifah DHH, Hozzein WN, Batiha GE-S, El Nahhas N, Mabrok MA, Infect. Drug Resist. 2020, 13, 3255. [PubMed: 33061472]

[8]. Dickey SW, Cheung GY, Otto M, Nat. Rev. Drug Discov. 2017, 16, 457. [PubMed: 28337021]

[9]. Kroll AV, Jiang Y, Zhou J, Holay M, Fang RH, Zhang L, Adv. Biosyst. 2019, 3, 1800219. [PubMed: 31728404]

[10]. Yenkoidiok-Douti L, Jewell CM, ACS Biomater. Sci. Eng. 2020, 6, 759. [PubMed: 33313391]

[11]. Zhou J, Kroll AV, Holay M, Fang RH, Zhang L, Adv. Mater. 2020, 32, 1901255.

[12]. Fang RH, Kroll AV, Gao W, Zhang L, Adv. Mater. 2018, 30, 1706759.

[13]. Hu C-MJ, Fang RH, Copp J, Luk BT, Zhang L, Nature Nanotechnol 2013, 8, 336. [PubMed: 23584215]

[14]. Thamphiwatana S, Angsantikul P, Escajadillo T, Zhang Q, Olson J, Luk BT, Zhang S, Fang RH, Gao W, Nizet V, Proc. Natl. Acad. Sci. U.S.A. 2017, 114, 11488. [PubMed: 29073076]

[15]. Zhang Q, Dehaini D, Zhang Y, Zhou J, Chen X, Zhang L, Fang RH, Gao W, Zhang L, Nat. Nanotechnol. 2018, 13, 1182. [PubMed: 30177807]

[16]. Hu C-MJ, Fang RH, Luk BT, Zhang L, Nat. Nanotechnol. 2013, 8, 933. [PubMed: 24292514]

[17]. Jones RG, Liu Y, Rigsby P, Sesardic D, Immunol J. Methods 2008, 337, 42.

[18]. Donald RG, Flint M, Kalyan N, Johnson E, Witko SE, Kotash C, Zhao P, Megati S, Yurgelonis I, Lee PK, Microbiology 2013, 159, 1254. [PubMed: 23629868]

[19]. Guo Z, Kubiatowicz LJ, Fang RH, Zhang L, Adv. Ther. 2021, 4, 2100072.

[20]. Zhang Y, Tu J, Wang D, Zhu H, Maity SK, Qu X, Bogaert B, Pei H, Zhang H, Adv. Mater. 2018, 30, 1703658.

[21]. Scharner J, Aznarez I, Mol. Ther. 2021, 29, 540. [PubMed: 33359792]

[22]. Guéry L, Dubrot J, Lippens C, Brighouse D, Malinge P, Irla M, Pot C, Reith W, Waldburger J-M, Hugues S, Cancer Res. 2014, 74, 6430. [PubMed: 25252912]

[23]. Shao Y, Sun Z-Y, Wang Y, Zhang B-D, Liu D, Li Y-M, ACS Appl. Mater. Interfaces 2018, 10, 9310. [PubMed: 29484882]

[24]. Bröker BM, Mrochen D, Péton V, Pathogens 2016, 5, 31. [PubMed: 26999219]

[25]. Bagnoli F, Fontana MR, Soldaini E, Mishra RP, Fiaschi L, Cartocci E, Nardi-Dei V, Ruggiero P, Nosari S, De Falco MG, Proc. Natl. Acad. Sci. U.S.A. 2015, 112, 3680. [PubMed: 25775551]

[26]. Huang Y, Xu W, Liu G, Tian L, Chem. Commun. 2017, 53, 3038.

[27]. Lin LY, McCarthy S, Powell BM, Manurung Y, Xiang IM, Dean WL, Chaires B, Yatsunyk LA, PLoS One 2020, 15, e0241513. [PubMed: 33206666]

[28]. Merindol R, Delechiave G, Heinen L, Catalani LH, Walther A, Nat. Commun. 2019, 10, 528. [PubMed: 30705271]

[29]. Chen MH, Wang LL, Chung JJ, Kim YH, Atluri P, Burdick JA, ACS Biomater. Sci. Eng. 2017, 3, 3146. [PubMed: 29250593]

[30]. Wang F, Gao W, Thamphiwatana S, Luk BT, Angsantikul P, Zhang Q, Hu CM, Fang RH, Copp JA, Pornpattananangkul D, Lu W, Zhang L, Adv. Mater. 2015, 27, 3437. [PubMed: 25931231]

[31]. Radovic-Moreno AF, Chernyak N, Mader CC, Nallagatla S, Kang RS, Hao L, Walker DA, Halo TL, Merkel TJ, Rische CH, Proc. Natl. Acad. Sci. U.S.A. 2015, 112, 3892. [PubMed: 25775582]

[32]. Buss CG, Bhatia SN, Proc. Natl. Acad. Sci. U.S.A. 2020, 117, 13428. [PubMed: 32493746]

[33]. Krieg AM, Nat. Rev. Drug Discov. 2006, 5, 471. [PubMed: 16763660]

[34]. Blazar BR, Krieg AM, Taylor PA, Blood 2001, 98, 1217. [PubMed: 11493473]

[35]. Stebegg M, Kumar SD, Silva-Cayetano A, Fonseca VR, Linterman MA, Graca L, Front. Immunol. 2018, 9, 2469. [PubMed: 30410492]

[36]. Shepherd FR, McLaren JE, Int. J. Mol. Sci. 2020, 21, 6144. [PubMed: 32858901]

[37]. Damsker JM, Hansen AM, Caspi RR, Ann. N. Y. Acad. Sci. 2010, 1183, 211. [PubMed: 20146717]

[38]. Wang F, Fang RH, Luk BT, Hu CMJ, Thamphiwatana S, Dehaini D, Angsantikul P, Kroll AV, Pang Z, Gao W, Adv. Funct. Mater. 2016, 26, 1628. [PubMed: 27325913]

[39]. Li Causi E, Parikh SC, Chudley L, Layfield DM, Ottensmeier CH, Stevenson FK, Di Genova G, PLoS One 2015, 10, e0136717. [PubMed: 26332995]

[40]. Pais Ferreira D, Silva JG, Wyss T, Fuertes Marraco SA, Scarpellino L, Charmoy M, Maas R, Siddiqui I, Tang L, Joyce JA, Delorenzi M, Luther SA, Speiser DE, Held W, Immunity 2020, 53, 985. [PubMed: 33128876]

[41]. Weisel NM, Joachim SM, Smita S, Callahan D, Elsner RA, Conter LJ, Chikina M, Farber DL, Weisel FJ, Shlomchik MJ, Nat. Immunol. 2022, 23, 135. [PubMed: 34937918]

[42]. Chan LC, Rossetti M, Miller LS, Filler SG, Johnson CW, Lee HK, Wang H, Gjertson D, Fowler VG Jr., Reed EF, Yeaman MR, Group MSI, Proc. Natl. Acad. Sci. U.S.A. 2018, 115, E11111. [PubMed: 30297395]

[43]. Jiang Y, Krishnan N, Heo J, Fang RH, Zhang L, Control J. Release 2020, 324, 505.

[44]. Lavrador P, Esteves MR, Gaspar VM, Mano JF, Adv. Funct. Mater. 2021, 31, 2005941.

[45]. Zhou J, Krishnan N, Guo Z, Ventura CJ, Holay M, Zhang Q, Wei X, Gao W, Fang RH, Zhang L, Sci. Adv. 2022, 8, eabq5492. [PubMed: 36083909]

[46]. Zhou J, Ventura CJ, Yu Y, Gao W, Fang RH, Zhang L, Nano Lett. 2022, 22, 7057. [PubMed: 35998891]

[47]. Lee JB, Peng S, Yang D, Roh YH, Funabashi H, Park N, Rice EJ, Chen L, Long R, Wu M, Luo D, Nat. Nanotechnol. 2012, 7, 816. [PubMed: 23202472]

[48]. Conde J, Oliva N, Atilano M, Song HS, Artzi N, Nat. Mater. 2016, 15, 353. [PubMed: 26641016]

[49]. Kroll AV, Fang RH, Jiang Y, Zhou J, Wei X, Yu CL, Gao J, Luk BT, Dehaini D, Gao W, Zhang L, Adv. Mater. 2017, 29, 1703969.

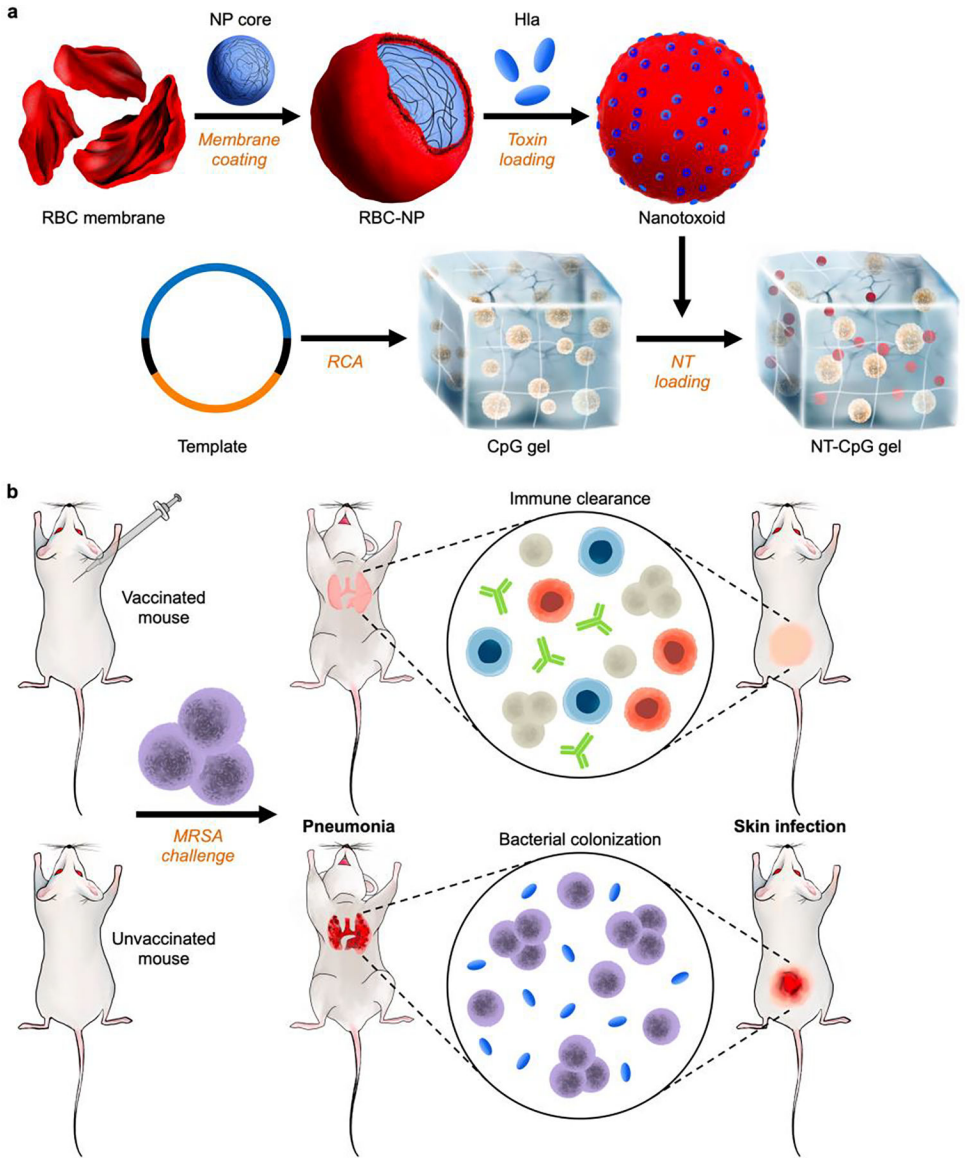

Figure 1.

Nanotoxoids embedded in an immunostimulatory DNA hydrogel for antibacterial vaccination. a) To fabricate nanotoxoids, staphylococcal α-hemolysin (Hla) is embedded into RBC membrane-coated nanoparticles (RBC-NPs). A DNA-based hydrogel with CpG 1826 repeats (CpG gel) is formed by rolling circle amplification (RCA). After loading nanotoxoids into a CpG gel, the resulting NT-CpG gel formulation can be used for antibacterial vaccination. b) Mice vaccinated with NT-CpG gel exhibit strong antibacterial immunity that protects them against MRSA pneumonia and skin infection.

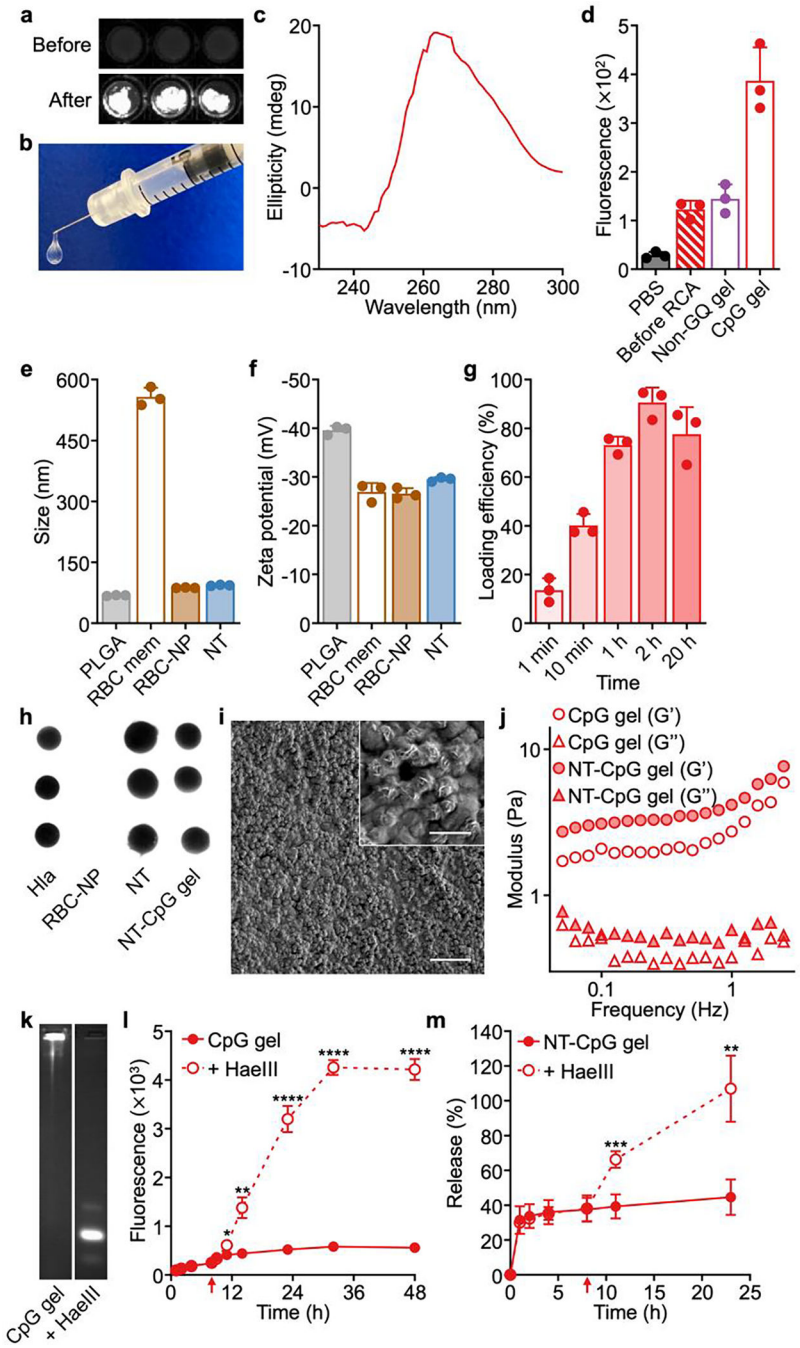

Figure 2.

NT-CpG gel preparation and characterization. a) Fluorescent visualization of GelRed-stained CpG gel reagent mixtures before or after the RCA process. b) Image showing a CpG gel passing through a 29-gauge needle. c) Circular dichroism spectrum of a CpG gel. d) Fluorescence of *N*-methyl mesoporphyrin IX incubated with PBS, a CpG gel reagent mixture before RCA, a non-G-quadruplex (non-GQ) CpG gel, and a CpG gel (n = 3, mean + SD). e,f) Particle size (e) and surface zeta potential (f) of PLGA cores, RBC membrane (RBC mem), RBC-NPs, and nanotoxoids (NT) as measured by dynamic light scattering (n =

3, mean + SD). g) Percentage of inputted nanotoxoids loaded into a CpG gel after increasing periods of incubation (n = 3, mean + SD). h) Dot blots probing for Hla on purified Hla, RBC-NPs, nanotoxoids (NT), and an NT-CpG gel. i) Scanning electron microscopy images of an NT-CpG gel. Scale bar = 2 μm (500 nm for the inset). j) Rheological analysis of a CpG gel and an NT-CpG gel measuring the storage modulus (G') and loss modulus (G'') as a function of frequency. k) Fluorescent visualization of a CpG gel with or without HaeIII treatment after electrophoresis on a 3% agarose gel. l) Degradation of a GelRed-stained CpG gel in PBS at 37 °C over time with or without the addition of HaeIII at 8 h (n = 3, mean ± SD). m) Release kinetics of nanotoxoids from an NT-CpG gel with or without the addition of HaeIII at 8 h (n = 4, mean ± SD). *$p < 0.05$, **$p < 0.01$, ***$p < 0.001$, and ****$p < 0.0001$. Statistical analysis was performed using a Student's unpaired *t*-test in (l,m).

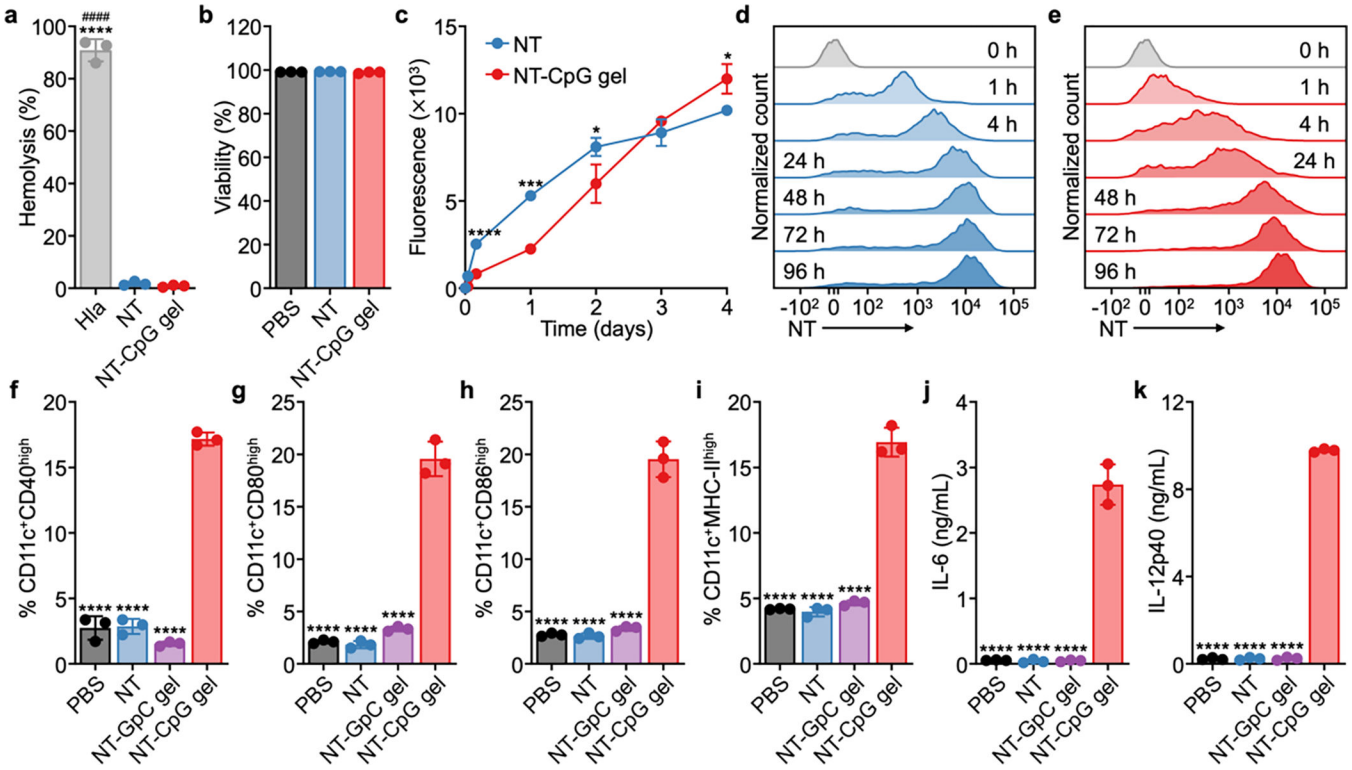

Figure 3.

In vitro biological characterization of NT-CpG gel. a) Hemolysis of RBCs treated with purified Hla, nanotoxoids (NT), and an NT-CpG gel (n = 3, mean + SD). b) Viability of BMDCs treated with nanotoxoids (NT) and an NT-CpG gel (n = 3, mean + SD). c-e) Uptake kinetics (c) of nanotoxoids (NT) in free form (d) or in an NT-CpG gel (e) by BMDCs over time (n = 3, mean ± SD). f-i) Expression of the maturation markers CD40 (f), CD80 (g), CD86 (h), and MHC-II (i) on $CD11c^{+}F4/80^{-}$ BMDCs 48 h after treatment with nanotoxoids (NT), an NT-GpC gel, and an NT-CpG gel (n = 3, mean + SD). j,k) Secretion of the proinflammatory cytokines IL-6 (j) and IL-12p40 (k) by BMDCs 48 h after treatment with nanotoxoids (NT), an NT-GpC gel, and an NT-CpG gel (n = 3, mean + SD). $^{*}p < 0.05$, $^{***}p < 0.001$, and $^{****}p < 0.0001$ (compared to NT-CpG gel); $^{\#\#\#\#}p < 0.0001$ (compared to NT). Statistical analysis was performed using a Student's unpaired *t*-test in (c) and ordinary one-way ANOVA with Tukey's multiple comparison's test in (a,f-k).

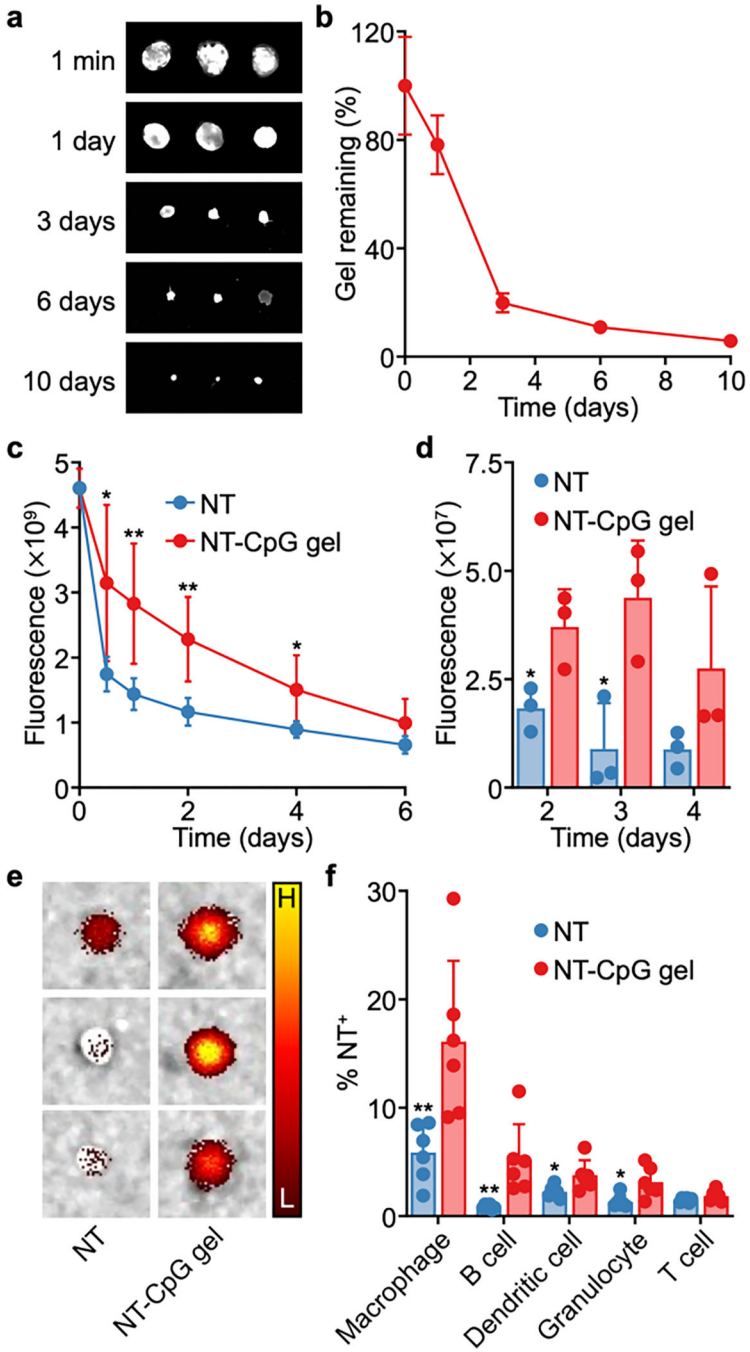

Figure 4.

In vivo characterization of NT-CpG gel. a,b) Fluorescent visualization (a) and quantification (b) of GelRed-labeled NT-CpG gels injected subcutaneously into mice and recovered at increasing intervals (n = 3, mean ± SD). c) Retention of nanotoxoids (NT) subcutaneously administered into the flank in free form and in an NT-CpG gel over time (n = 6, mean ± SD). d,e) Quantification (d) and imaging (e) of NT in the draining lymph nodes after subcutaneous administration into the hock in free form and in an NT-CpG gel (n = 3, mean + SD); H: high signal, L: low signal. f) Percentage of various cell populations in the draining

lymph node positive for NT uptake after subcutaneous administration of NT into the hock in free form and in an NT-CpG gel (n = 6, mean + SD). *$p < 0.05$ and **$p < 0.01$. Statistical analysis was performed using a Student's unpaired *t*-test in (c,d,f).

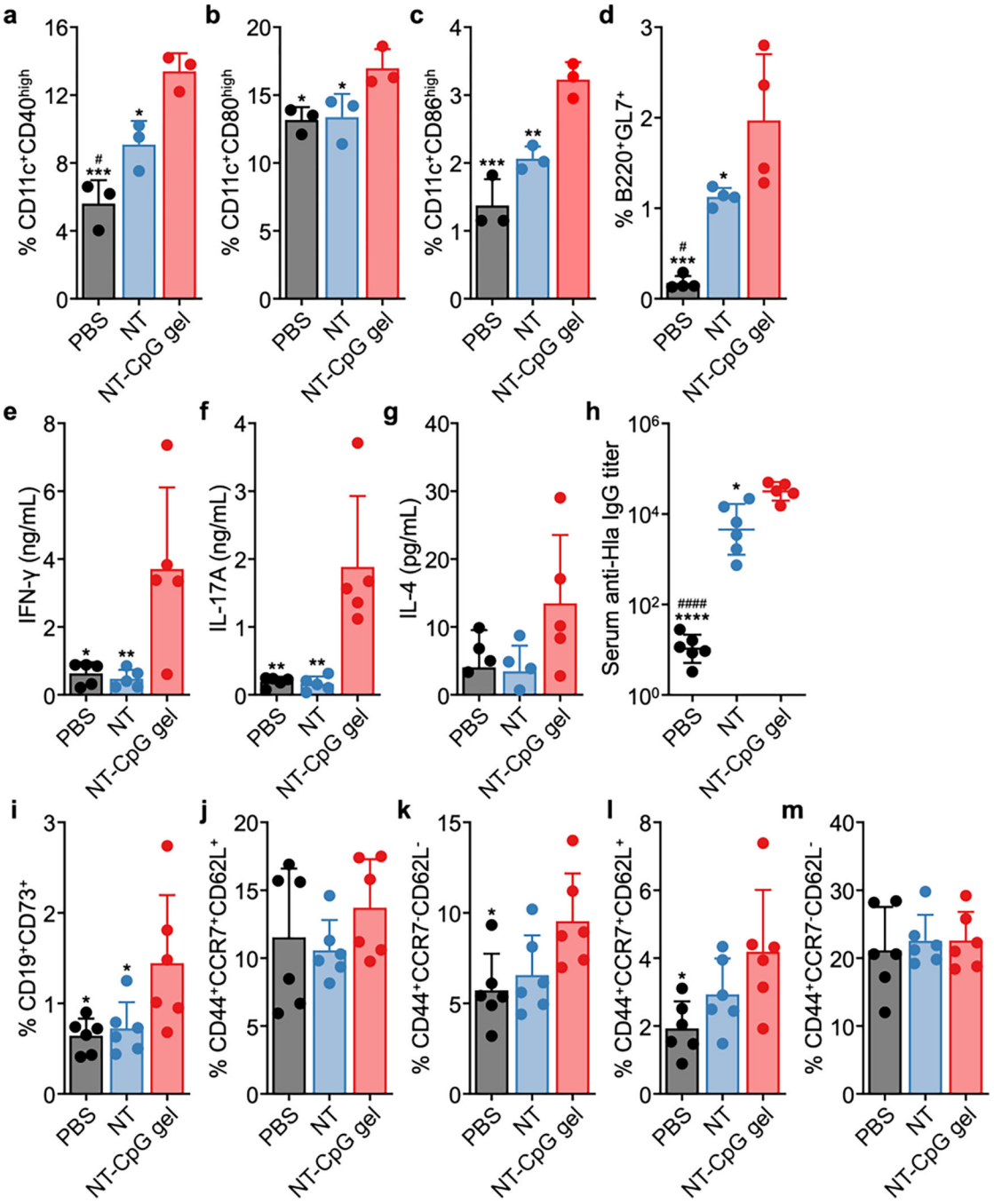

Figure 5.

In vivo immune responses. a-c) Expression of the maturation markers CD40 (a), CD80 (b), and CD86 (c) on $CD11c^{+}F4/80^{-}$ dendritic cells in the draining lymph nodes 48 h after hock injection with nanotoxoids (NT) or an NT-CpG gel (n = 3, mean + SD). d) Quantification of $B220^{+}GL7^{+}$ germinal center B cells in the draining popliteal lymph nodes 21 days after hock injection with nanotoxoids (NT) or an NT-CpG gel (n = 4, mean + SD). e-g) Production of the cytokines IFN-γ (e), IL-17A (f), and IL-4 (g) by splenocytes collected 28 days after vaccination with nanotoxoids (NT) or an NT-CpG gel, followed by stimulation

with Hla for 5 days (n = 5, mean + SD). h) Anti-Hla IgG titers in the serum 35 days after vaccination with nanotoxoids (NT) or an NT-CpG gel (n = 5 for NT-CpG gel, n = 6 for PBS and NT, mean ± SD). i) Memory B cells in the $CD45^+$ cell population in the draining lymph node 28 days after vaccination with NT or an NT-CpG gel (n = 6, mean + SD). j-m) Central memory (j,l) and effector memory (k,m) T cells within the $CD45^+CD4^+$ (j,k) and $CD45^+CD8^+$ (l,m) cell populations in the draining lymph node 28 days after vaccination with NT or an NT-CpG gel (n = 6, mean + SD). $^*p < 0.05$, $^{**}p < 0.01$, $^{***}p < 0.001$, and $^{****}p < 0.0001$ (compared to NT-CpG gel); $^{\#}p < 0.05$ and $^{\#\#\#\#}p < 0.0001$ (compared to NT). Statistical analysis was performed using ordinary one-way ANOVA with Tukey's multiple comparison's test in (a-h,i,k,l).

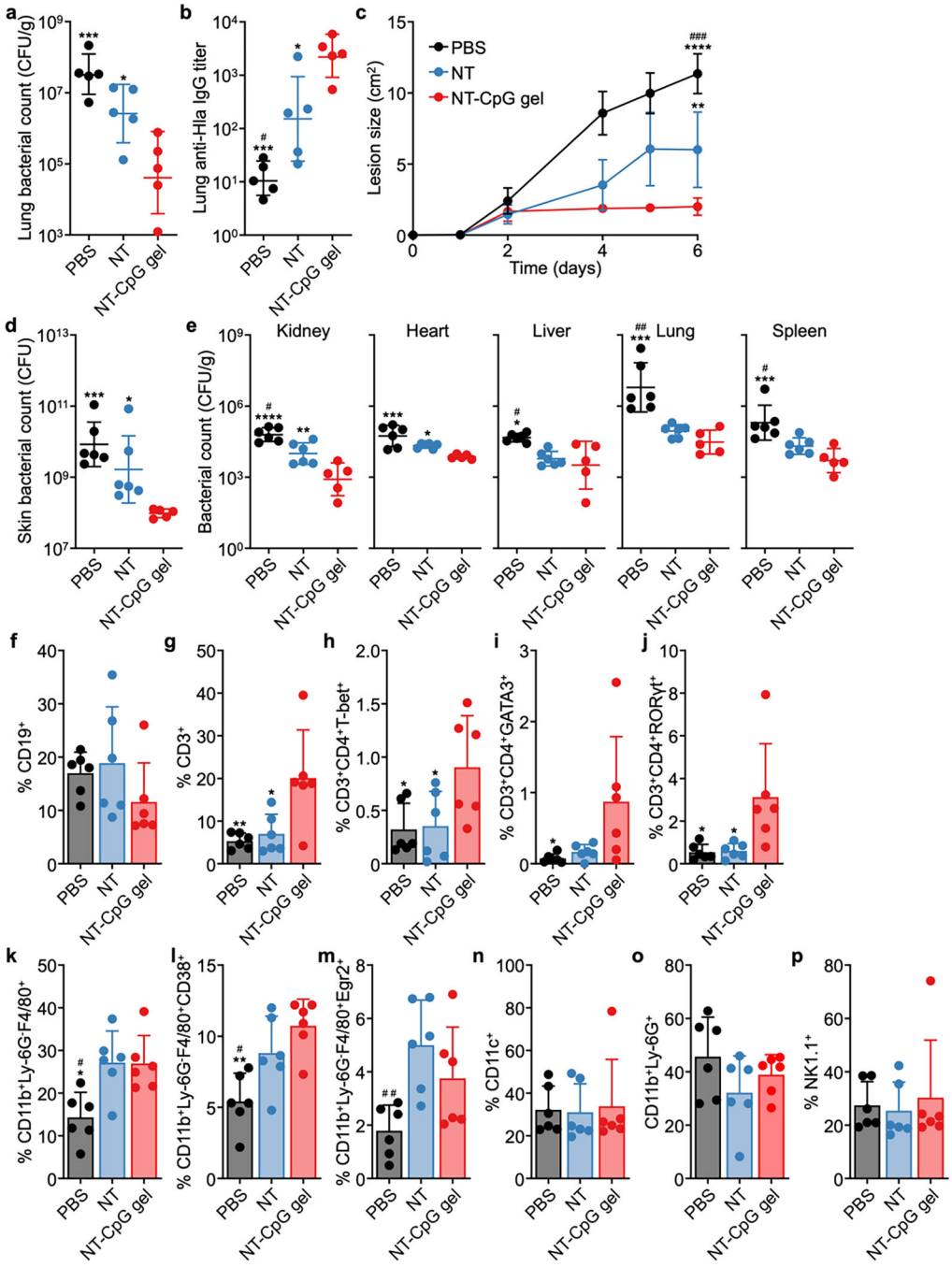

Figure 6.

In vivo protective efficacy against live MRSA challenge. a,b) Bacterial counts (a) and anti-Hla IgG titers (b) in the lungs of mice 24 h after intratracheal MRSA challenge on day 35 after vaccination with nanotoxoids (NT) or an NT-CpG gel (n = 5, mean ± SD). c-e) Lesion area over time (c), as well as skin (d) and organ (e) bacterial counts 6 days post challenge, of mice subcutaneously challenged with MRSA on day 35 after vaccination with nanotoxoids (NT) or an NT-CpG gel (n = 5 for NT-CpG gel, n = 6 for PBS and NT, mean ± SD). f-p) B cells (f), T cells (g), Th1 cells (h), Th2 cells (i), Th17 cells (j), macrophages (k),

M1 macrophages (l), M2 macrophages (m), dendritic cells (n), neutrophils (o), and natural killer cells (p) in the $CD45^+$ cell population in the infected skin tissue of mice 3 days after subcutaneous MRSA challenge on day 21 after vaccination with nanotoxoids (NT) or an NT-CpG gel (n = 6, mean + SD). *$p < 0.05$, **$p < 0.01$, ***$p < 0.001$, and ****$p < 0.0001$ (compared to NT-CpG gel); $^{\#}p < 0.05$, $^{\#\#}p < 0.01$, and $^{\#\#\#}p < 0.001$ (compared to NT). Statistical analysis was performed using ordinary one-way ANOVA with Tukey's multiple comparison's test in (a-e, g-m).